



**HAL**  
open science

## 3D Reconstruction of the Proximal Femur Shape from Few Pairs of X-Ray Radiographs

Sonia Akkoul, Adel Hafiane, Olivier Rozenbaum, Eric Lespessailles, Rachid Jennane

► **To cite this version:**

Sonia Akkoul, Adel Hafiane, Olivier Rozenbaum, Eric Lespessailles, Rachid Jennane. 3D Reconstruction of the Proximal Femur Shape from Few Pairs of X-Ray Radiographs. *Signal Processing: Image Communication*, 2017, 59, pp.65-72. 10.1016/j.image.2017.03.014 . insu-01502999

**HAL Id: insu-01502999**

**<https://insu.hal.science/insu-01502999v1>**

Submitted on 8 Apr 2017

**HAL** is a multi-disciplinary open access archive for the deposit and dissemination of scientific research documents, whether they are published or not. The documents may come from teaching and research institutions in France or abroad, or from public or private research centers.

L'archive ouverte pluridisciplinaire **HAL**, est destinée au dépôt et à la diffusion de documents scientifiques de niveau recherche, publiés ou non, émanant des établissements d'enseignement et de recherche français ou étrangers, des laboratoires publics ou privés.



Distributed under a Creative Commons Attribution - NonCommercial - NoDerivatives 4.0 International License

# Author's Accepted Manuscript

## 3D Reconstruction of the Proximal Femur Shape from Few Pairs of X-Ray Radiographs

Sonia Akkoul, Adel Hafiane, Olivier Rozenbaum, Eric Lespessailles, Rachid Jennane



PII: S0923-5965(17)30049-8  
DOI: <http://dx.doi.org/10.1016/j.image.2017.03.014>  
Reference: IMAGE15198

To appear in: *Signal Processing : Image Communication*

Received date: 29 February 2016  
Revised date: 3 February 2017  
Accepted date: 22 March 2017

Cite this article as: Sonia Akkoul, Adel Hafiane, Olivier Rozenbaum, Eric Lespessailles and Rachid Jennane, 3D Reconstruction of the Proximal Femur Shape from Few Pairs of X-Ray Radiographs, *Signal Processing : Image Communication*, <http://dx.doi.org/10.1016/j.image.2017.03.014>

This is a PDF file of an unedited manuscript that has been accepted for publication. As a service to our customers we are providing this early version of the manuscript. The manuscript will undergo copyediting, typesetting, and review of the resulting galley proof before it is published in its final citable form. Please note that during the production process errors may be discovered which could affect the content, and all legal disclaimers that apply to the journal pertain.

# 3D Reconstruction of the Proximal Femur Shape from Few Pairs of X-Ray Radiographs

Sonia Akkoul<sup>1</sup>, Adel Hafiane<sup>2</sup>, Olivier Rozenbaum<sup>3</sup>, Eric Lespessailles<sup>4,5</sup> and Rachid Jennane<sup>5</sup>

<sup>1</sup>Univ. Orléans, PRISME, EA4229, 12 rue de Blois, 45067 Orléans, France

<sup>2</sup>INSA Centre Val de Loire, PRISME, EA 4229, 88, Av. Lahitolle, 18020 Bourges, France

<sup>3</sup>Univ. Orléans, ISTO, UMR 7327, 1A, rue de la Férollerie, 45071 Orléans, France

<sup>4</sup>Nouvel Hôpital d'Orléans, Service de Rhumatologie, 45032 Orléans, France

<sup>5</sup>Univ. Orléans, I3MTO, EA 4708, 5 rue de Chartres, 45067 Orléans, France

Sonia.Akkoul@univ-orleans.fr

## Abstract

This paper presents a 3D reconstruction method of the proximal femur shape based on contour identification from pairs of 2D X-ray radiographs. The aim is to reconstruct the 3D surface of the proximal femur from a limited number of projections. Our approach is based on the reconstruction of several 3D contours, which are meshed to obtain a 3D shape. Our proposed algorithm is based on different processing steps to obtain the 3D personalized model. Three approaches are proposed. The first technique consists of contour extraction, matching the points of these contours and calculation of a 3D contour using an original algorithm. The second and third techniques use the results of the previous method as well as new points chosen by an operator from a reference model of femur to improve accuracy either globally or only in sensitive areas. The proposed method was evaluated on 10 cadaveric proximal femurs using the 3D CT-Scan models. Obtained results show good performance and promising perspectives for 3D shape reconstruction of the femur from only a few pairs of radiographs.

**Keywords:** 3D shape reconstruction, stereo-radiography, proximal femur.

## 1. INTRODUCTION

Personalized three dimensional (3D) patient bone models provide an interesting analysis tool for the diagnosis and the follow-up of many bone diseases and play an important role in pre-operative surgery planning and improved guidance during surgical interventions such as total hip replacement, modeling and simulation.

Accurate 3D anatomical models can be achieved using conventional 3D imaging modalities such as Computed Tomography (CT-Scan) and Magnetic Resonance Imaging (MRI). However, the use of these modalities is restricted to few specific procedures, due to constraints of radiation risk, cost and availability. In addition, the majority of these modalities require the patient to be lying down, thus involving a lengthy acquisition protocol with a positioning, which does not allow clinical evaluation of physiological function.

Thus, the diagnosis and planning of many interventions still rely on two-dimensional radiographic images, where the surgeon has to mentally visualize the 3D anatomy of interest.

As an alternative to current 2D radiographs, direct 3D imaging needs to be developed in order to assist clinicians in their medical tasks [1]. However, reconstructing a 3D bone shape from a small number of 2D X-ray images is a challenging problem, especially when reconstructing a patient bone specific surface model.

Studies on the reconstruction of bone models based on information collected through 2D imaging modalities can be divided into two groups: methods that use only 2D images for 3D model reconstruction [2] and methods based on prior knowledge of the 3D anatomical structure in addition to 2D images [1]. Most of these studies require prior knowledge of the 3D anatomy model to compensate for the lack of information obtainable from the 2D images [1]. This information can be provided by incorporating a generic geometrical shape of the bone structure [3], [4], [27], by Statistical Shape Models (SSM) [5], [6], [7], [28], by Parametric Models [8], [9], [10], or by using independent shape and appearance models that are learned from a set of training data to encode the information of the bone [29]. To reduce radiation exposure, some authors have proposed 3D reconstruction methods from bi-planar X-ray images based on stereovision techniques [4], [11], [12]. Our work is based on the same principle, i.e. to propose an alternative method using pairs of X-ray images taken in an upright position.

Our proposed approach for the 3D proximal femur surface reconstruction is based on a pseudo stereo matching technique. An original mathematical model and a limited number of

2D X-ray images taken from different orientations are employed for this purpose. The proposed scheme comprises two main stages. In the first one, two successive projections are used to compute the coordinates of a 3D contour. After extracting the contour of the proximal femur from the 2D X-ray images, the matching process is carried out. To match the points of two contours, three distances were compared: the City-block, the Chess board and the Euclidian 2D spatial distances. The estimated point pairs are then used to compute a set of 3D points. The surface model is reconstructed from this cloud of points by a meshing technique based on Poisson's equation which enables a closed 3D surface to be obtained. In the second stage, a 3D reference surface of the proximal femur is used to extract points and inject them locally into the reconstructed surface to compensate for the lack of information and improve the accuracy of the reconstructed 3D surface. To assess the accuracy of the proposed shape reconstruction framework, our results are compared to real 3D CT-scan data. Ten cadaveric proximal femurs were used as the anatomy of interest throughout this study.

The paper is organized as follows: Section 2 explains the method and the proposed projection model. Section 3 presents the data, reports the experimental results and presents the global and local correction shape methods. The last section concludes this paper.

## **2. PROPOSED METHOD**

This section aims to describe the proposed method for the 3D reconstruction of the femur from CT scanner images. The projection model and the different processing steps are presented.

### **2.1 The 3D model**

The protocol of acquiring the radiographic images is shown in Figure 1. The proximal femur is placed between the X-ray source and the rotating sensor. An X-ray of the specimen is acquired at each angle  $\alpha$ .

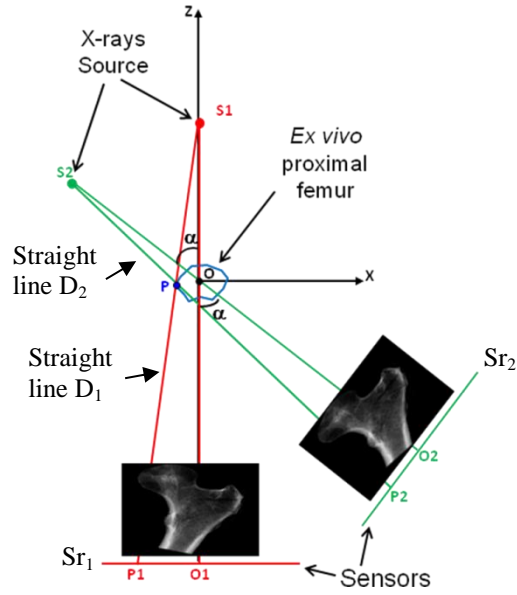


**Figure 1:** Data acquisition process.

Let the pairs of points  $(P1, O1)$  and  $(P2, O2)$  represent the projection of a point  $P$  of the object and the projection of the center of rotation  $O$  on the sensor before and after rotation, respectively. From the coordinates of the points  $P1$  and  $P2$  and using our proposed mathematical model (detailed in Section 2.2), the 3D coordinates of the point  $P$  can be determined.

Since our aim is to use a minimum number of radiographic images, it was necessary to assess the impact of the choice of the angle between two radiographs as well as the influence of the angle between two pairs of radiographs on the quality and the accuracy of the 3D reconstructed shape. To do so, the angle  $\alpha$  between two images of the same pair was fixed at 4 degrees and the angle  $\beta$  between the pairs of radiographs was set at different values (10, 20, 30, 45 and 60 degrees). For each angle  $\beta$ , the error between the 3D reconstructed shape and the ground truth was estimated and the optimal orientation  $\beta_o$  giving the minimum error was retained. Keeping the angle  $\beta_o$ , the next step consisted in varying the angle  $\alpha$  from 4 to 32 degrees by power of 2, in order to find the best combination  $(\alpha_o, \beta_o)$  that reconstructs the desired 3D shape close to the ground truth (GT) [14]. Figure 2 illustrates different pairs of X-ray projections separated by the angles  $\alpha$  and  $\beta$ .

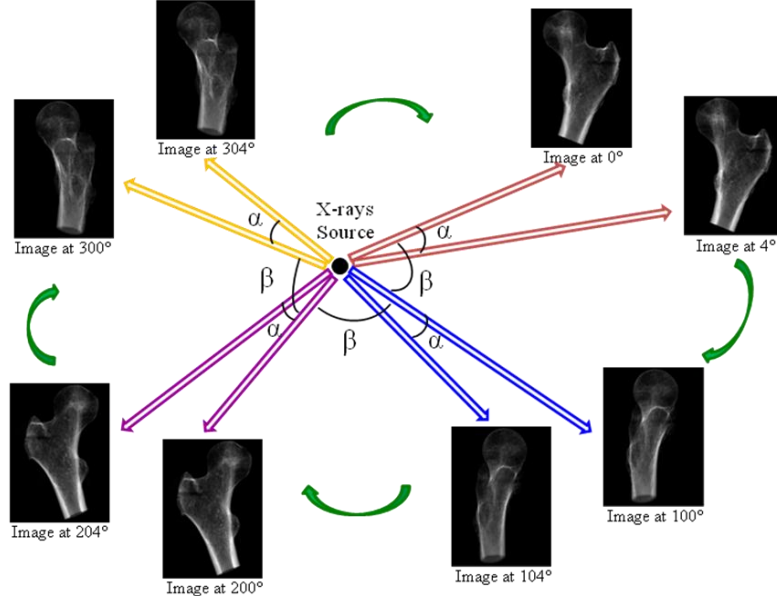


**Figure 2:** Illustration of the angle  $\beta$  between two pairs of radiographs as well as the angle  $\alpha$  between two radiographs of the same pair. For this example,  $\alpha = 4$  and  $\beta = 100$  degrees.

## 2.2 Computing 3D points

This section describes how the 3D coordinates are computed from the 2D points selected [15]. Using the diagram in Figure 1, the bone is placed between the source and the sensor, the Y-coordinate (height) is fixed, and the source and the sensor are rotated around the object along the Y axis.

Let  $R(X, Z)$  be the reference system and  $P_1$  (with  $(P_{1x}, P_{1y})$  as coordinates), the projection onto the sensor of the point  $P$ . Knowing the distance between the X-ray source  $S_1$  and the sensor  $S_{r1}$ , and the distance between the bone and the source and using the Thales theorem it is possible to calculate the Y coordinate of the point  $P$  (Figure 3).

To compute the Y coordinate one can use:

$$\frac{OS_1}{O_1S_1} = \frac{Y}{P_{1y}} \Rightarrow Y = \frac{OS_1}{O_1S_1} * P_{1y} \quad (1)$$

Once the Y coordinate has been calculated, the resolution of the system of two equations obtained using the straight lines  $(S_1P_1)$  and  $(S_2P_2)$  (Figure 1) is used to calculate the coordinates X and Z.

The first equation represents the straight line  $D_1$  (Figure 1) connecting the X-ray source  $S_1$  to the point  $P_1$  which represents the projection of the point  $P$  on the sensor before rotation of the source-sensor system.

$$Z = \frac{-OO_1 - OS_1}{P_{1x}} X + OS_1 \quad (2)$$

where  $OO_1$  is the distance between the bone and the sensor,  $OS_1$  is the distance between the bone and the X-ray source, and  $P_{1x}$  is the X coordinate of the projected point  $P$  on the sensor.

The second equation shows the same straight line  $D_1$  linking the X-ray source and the sensor through the point  $P$  after rotation of the source-sensor system by an angle  $\alpha$ . As the object and source-sensor distances are fixed, the source-object and object-sensor distances are invariant. Thus, we obtain:

$$OO_1 = OO_2 \text{ and } OS_1 = OS_2 \quad (3)$$

The equation of the second straight line  $D_2$  (Figure 1) can then be written as follows:

$$Z = \frac{-OO_1 * \cos\alpha - P_2x * \sin\alpha - OS_1 * \cos\alpha}{OO_1 * \sin\alpha - P_2x * \cos\alpha + OS_1 * \sin\alpha} X + C \quad (4)$$

with,

$$C = OS_1 * \cos\alpha - \frac{-OO_1 * \cos\alpha - P_2x * \sin\alpha - OS_1 * \cos\alpha}{OO_1 * \sin\alpha - P_2x * \cos\alpha + OS_1 * \sin\alpha} * (-OS_1 * \sin\alpha) \quad (5)$$

Substituting equation (10) in equation (9),  $Z$  can be written as:

$$Z = \gamma * X + (OS_1 * \cos\alpha) + \gamma * (OS_1 * \sin\alpha) \quad (6)$$

with,

$$\gamma = \frac{-OO_1 * \cos\alpha - P_2x * \sin\alpha - OS_1 * \cos\alpha}{OO_1 * \sin\alpha - P_2x * \cos\alpha + OS_1 * \sin\alpha} \quad (7)$$

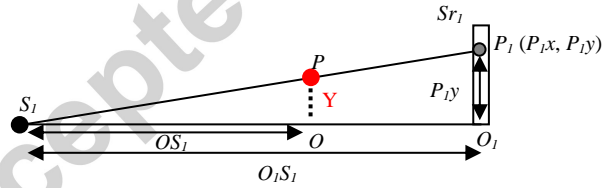


**Figure 3:** Calculation of the Y coordinate using the Thales theorem.

where  $S_1$  is the X-ray Source,  $Sr_1$  is the Sensor,  $P$  is a point of space belonging to the object,  $P_1 (P_{1x}, P_{1y})$  is the projection of the point  $P$  on the sensor,  $OS_1$  is the source-object distance and  $O_1S_1$  is the sensor-source distance.

The solution  $(X, Z)$  of the system of equations (2) and (4) is the coordinates of the point  $P$ . Thus, for each pair of projections separated by an angle  $\alpha$ , it is possible from these equations to estimate the coordinates of a 3D contour. Using several pairs of images, a 3D points cloud is obtained.



### 2.3. 3D reconstruction process

This section presents the processing flowchart (Figure 4) and the different steps of the proposed method for the 3D shape reconstruction of the proximal femur. After data acquisition, we extract the contours and match them by pairs. Then, using our proposed algorithm the 3D points are calculated, registered and meshed to generate the 3D shape form [15]. A description of each step is described in the following sections:

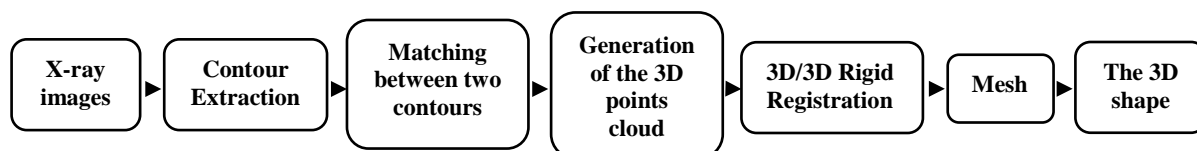


**Figure 4:** The proposed processing flowchart.

#### 2.3.1 Block based contour extraction

For edge detection, we used active contour models (ACM), because unlike conventional methods, active contours provide closed and smooth contours, which are suitable for our application. In addition, the contours are more regular and less sensitive to noise, because they are subjected to certain rigidity. To this end, we used the Chan and Vese [16] model. For the initialization step, different configurations were tested (square and circle), and the circle was retained, because it provides better convergence and better fitting of the contours. The initialization was done from the center of the image. The required parameters by the method (regularization and fitting parameters) were fixed empirically.

However, extracting the contours can be complex. In the case of radiographs taken at 90 degrees, for example, there is occlusion of different regions of the proximal femur. The great trochanter is superimposed to the intertrochanteric region. In this radiograph, the intertrochanteric area is the Region Of Interest (ROI) and when the edge detection method is applied on the entire image, it is the outer contour that is detected rather than the contour of the ROI (Figure 5.b).

To improve the contour detection, we divided the image into three blocks to isolate the great trochanter into the middle block and process each block independently. For our images, using ACM enabled obtaining precise contours. Thus, no post processing was needed to assemble the obtained contours. This way, it is possible to better define the area of interest and reduce occlusion effects. Figure 5.c shows the obtained result after subdivision of the image as shown in Figure 5.a.

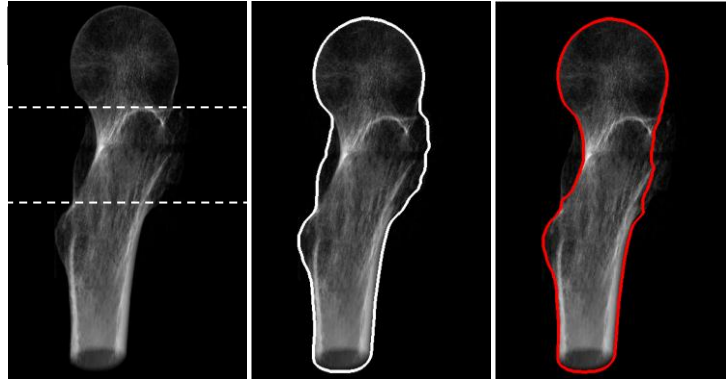


**Figure 5:** Improved contour detection. a) X-ray image taken at  $90^\circ$ . b) Obtained contour using the entire image. c) Obtained contour after subdivision of the image.

### 2.3.2. Matching between 2D contours

Once the 2D contours are extracted, matching procedure is applied to determine the 3D coordinates. The objective is to establish a correspondence between two input images from the same pair separated by an angle  $\alpha$ . For a given point on the first X-ray image, the goal is to identify a corresponding point on the second X-ray image [18]. Several techniques exist for matching contours [19], [20], [21]. For the present study, the matching between the points of two contours was performed by computing three different distances: the City-block, the Chess board and the Euclidian 2D spatial distance. Comparison of these three distances is presented in section 3.1.

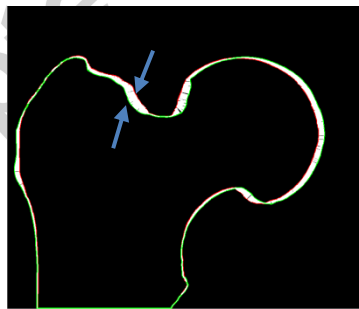


**Figure 6:** Extracted contours. (a) Contour1 (red), extracted contour from the first image, (b) Contour2 (green), extracted contour from the second image with a gap of  $\alpha = 4$  degrees.

Since we are using binary images, matching using contour 1 (C1) towards contour 2 (C2) is not symmetric and the points obtained may be different if C2 is used towards C1. Therefore, the 3D reconstruction shape may be different. To discuss this issue and study its influence on the 3D reconstructed shape, the following configurations were tested [15]:

- Configuration 1: C1 towards C2.
- Configuration 2: C2 towards C1.
- Configuration 3: the intersection between the results of configurations 1 and 2. Here the goal is to keep the pairs of pixels that are common to both configurations.
- Configuration 4: the union of the results of configurations 1 and 2. Here the goal is to keep the maximum number of pixel pairs.

The obtained results are presented in the experimental section (Section 3).

### 2.3.3. 3D rigid registration

Before meshing the obtained 3D point cloud, a rigid registration with a 3D point cloud extracted from the GT is needed. Using Meshlab, the 3D points cloud from the GT was extracted as a meshed surface. Then, all the vertexes were retained as 3D points cloud. Finally, by registering the 3D point cloud in the same environment as the GT, the error between the two surfaces can be estimated. For the registration, we used the Iterative Closest Point (ICP) algorithm [22], [23], [24], [31], which is employed to minimize the difference between two clouds of points. The first step of the ICP algorithm is based on the search for pairs of nearest points between the two sets (reconstructed and ground truth). The second step includes the estimation of the optimal rigid transformation that aligns the two data sets. In the last step, the rigid transformation is applied to the points of the reconstructed data. The procedure iteratively revises the transformations (translation, rotation) needed to minimize the distance between the points until convergence is achieved.

The registration step is followed by the meshing which enables reconstructing the 3D surface of the proximal femur.

### 2.3.4. Meshing

Next comes the meshing and the reconstruction of the computed 3D shape. This task was achieved using Meshlab [25] which is an advanced 3D software system for the processing and editing of unstructured 3D triangular meshes.

Our aim is to regularize surfaces and reduce noise and other artifacts, thus our choice focused on the Poisson surface reconstruction algorithm proposed in Meshlab. The method requires the 3D points cloud as well as their corresponding normals.

The computation of the normals requires 3 steps:

- "Locating tangent planes": makes it possible to find the tangent planes for the approximation of the local surface. For this, the center of gravity of each vertex of the triangles constituting the mesh is computed as the average of the set of the  $K$ -closest neighbors.
- "Building Riemannian graph": enables to construct the graph of Riemann, which helps creating the structure, where for each vertex, the borders of its closest  $K$ -neighbors are included in the construction.
- "Minimum spanning tree": applies the Kruskal's algorithm [30] on the Riemann graph to weight the normals.

To sum up, the algorithm computes the normal of a 3D point as a weighted product of its closest  $K$ -neighbors.

### 3. Experiments and results

Using a few X-ray image projections, our task is to extract 3D information and reconstruct the 3D shape of the femur. For this purpose, ten cadaveric proximal femurs (F1, F2, ..., F10) were completely scanned using a CT scanner. This imaging modality provides both the projections and the resulting 3D volume and avoids calibration of the input images. Two different devices were used for acquisition, with no impact on our proposed method for the reconstruction of the 3D proximal femur shape. X-Ray tomographic images of three proximal femurs (F1, F2 and F3) were obtained using a high quality Computed Tomography (CT) scanner (eXplore CT120). The specimens were imaged with an isotropic pixel size of 50  $\mu\text{m}$ . Each sample was placed between the X-ray source and the rotating sensor (Figure 1). The distance between the X-ray source and the sensor was 45.265 cm and each proximal femur was placed 39.776 cm from the source. The seven other proximal femurs (F4-F10) were scanned using the Nanotom (Phoenix) scanner with a resolution of 50  $\mu\text{m}$ . The distance between the X-ray source and the sensor was 50 cm and each proximal femur was placed 25 cm from the source. Thus, two different devices were used for acquisition, with no impact on our proposed method for the reconstruction of the 3D proximal femur shape.

The 3D volumes were reconstructed using an implementation based on Feldkamp's cone beam reconstruction algorithm [13]. Examples of the *ex vivo* proximal femur radiographs are shown in Figure 7 for different orientations ( $0^\circ$ ,  $90^\circ$ ,  $25^\circ$  and  $315^\circ$ ). The 3D models of the

reconstructed proximal femurs are used as ground truths to compare the performances of our proposed algorithm.

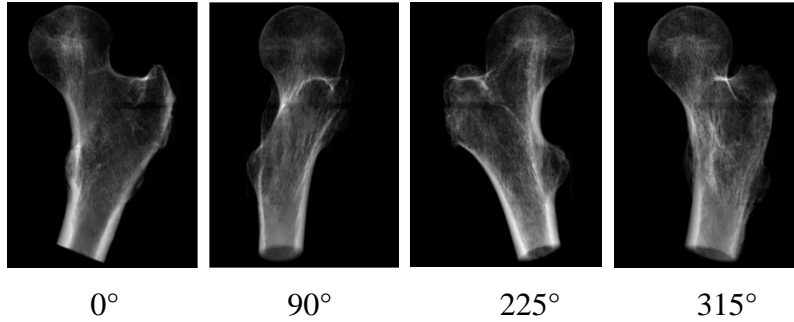


**Figure 7:** X-ray images of the *ex vivo* proximal femur at different orientations.

### 3.1. Influence of the contour matching distance

First, to validate our acquisition protocol and our proposed approach, one extra cadaveric sample (different from F1,... , F10) was used to fix the optimal distance and angles. After performing various tests, the results showed that the optimal angles for the 3D reconstruction of the proximal femur shape are  $(\alpha_o, \beta_o) = (4^\circ, 45^\circ)$  which led to use 16 projections.

For the matching of the contours, our processing chain was used to reconstruct the first 3D proximal femur with the three distances and the results were compared. The distance which gave the minimum error after the 3D reconstruction was selected. The comparison of the three distances showed that the Euclidean distance gives the best results (Table 1). It was therefore retained for the experiments in the present study.

**Table 1:** Estimated maximum, average and RMS errors for the three distances.

	City-block (mm)	Chess-board (mm)	Euclidean distance (mm)
Maximum Error	17.568	14.073	15.434
Mean Error	2.615	2.592	<b>2.528</b>
RMSE	3.758	3.556	<b>3.506</b>

Table 2 compares the results using the four configurations for the asymmetric distance presented in section 2.3.2. As can be seen, the contours matching of configuration 1 provides the minimum errors, whatever the used distance. This configuration is therefore better suited for our application.

The estimated point pairs are then used to compute a set of 3D points.

**Table 2:** Maximum error, Mean error and RMS obtained using the three distances and the four configurations.

	City Block (mm)			Chess Board (mm)			Euclidean Distance (mm)		
	Max Err	Mean Er	RMS	Max Err	Mean Er	RMS	Max Err	Mean Er	RMS
Conf. 1	17.568	<b>2.615</b>	<b>3.758</b>	14.073	2.592	<b>3.556</b>	15.434	<b>2.528</b>	<b>3.506</b>
Conf. 2	15.173	2.768	3.949	14.706	2.585	3.598	14.434	2.689	3.785
Conf. 3	13.898	2.856	3.933	13.980	3.154	4.170	15.454	3.053	4.151
Conf. 4	16.180	3.078	4.299	16.526	3.308	4.578	15.657	2.916	4.087

Once our approach have been validated, it was applied on the ten proximal femurs to test its robustness. The next section presents the obtained results.

### 3.2. Estimation of the error of reconstruction

For each sample, the optimal parameters for contour extraction, angles, etc. were settled. Figure 8 shows visual examples of the 3D surfaces obtained for different proximal femurs and the estimated errors compared to the GT. These errors were evaluated using the Metro tool on simplified surfaces [26]. The error is estimated in term of mean symmetric distance using the Euclidean distance to evaluate the difference between two triangular meshes. For this purpose, the “Point-to-surface distance” approach available in Metro was used.

The red and blue colors in the 3D reconstructed shapes represent the high and the low error values, respectively. For each sample, the low error value (blue color) is near the zero value, while the high error value is expressed by red color. Table 3, summarizes the reconstruction error of the ten proximal femurs. It noticed that, the errors obtained are mainly due to an occlusion effect which leads to poor edge detection and poor matching at the cavity between the femoral neck and the greater trochanter which is the most difficult area to rebuild.

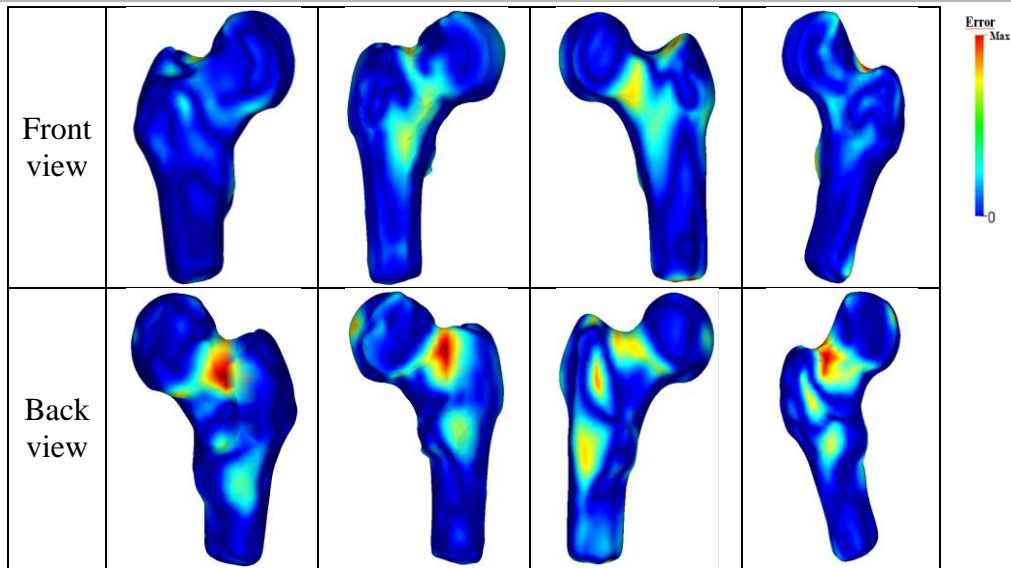


**Figure 8:** Reconstructed 3D surfaces for different proximal femurs and estimated errors using Metro with Euclidean distance. The low error value (equal to zero) correspond to the blue color, while the maximale error is represented in red.

Table 3 presents the maximum error, average error and RMSE (Root Mean Square Error) obtained for the 3D reconstructed proximal femurs. As can be seen, results demonstrate that whatever the processed sample (acquired using the different devices, eXplore CT or Nanotom), our approach gives stable and encouraging results with equivalent errors, demonstrating its robustness for 3D reconstruction.

**Table 3:** Estimated maximum, average and RMS errors for the ten proximal femurs.

Proximal femur	Maximum error (mm)	Mean error (mm)	RMS (mm)
F1	9.421	0.889	1.369
F2	9.237	1.259	1.753
F3	10.498	1.291	1.883
F4	10.490	0.940	1.441
F5	9.378	0.913	1.384
F6	9.657	1.344	1.784
F7	7.709	1.379	1.869
F8	7.740	1.327	1.859
F9	7.197	0.860	1.280
F10	8.001	0.926	1.283

The next section presents our proposed method to improve the obtained results.

### 3.3. Global and local shape correction

As shown in Table 3 and Figure 8 our approach enabled 3D reconstruction of the proximal femur surface with a satisfactory accuracy. However, a precise analysis of the results shows that there is some residual error in the upper part of the femoral neck on the side of the greater trochanter. The following sections present two new approaches to improve the reconstructed 3D shape and overcome the lack of information in this area.

#### 3.3.1 Global correction

To improve the 3D reconstructed shape, we propose to densify the reconstructed point cloud. The first attempt called global approach [15] consists in extracting a percentage of points randomly from a reference volume and injecting them into the shape to be reconstructed (Figure 9). The extraction of the points was achieved using Meshlab tool as a meshed surface. Then, all the vertexes were retained as 3D points cloud. The 3D Euclidean distance was used as a criterion between the points of the reference volume and those of the rebuilt cloud. To select only relevant points, *i.e.* points different from existing ones (already computed points), a threshold value on the number of points to retain was fixed. The threshold was chosen according to the percentage of points to be inserted in the 3D surface to be reconstructed. The percentage was calculated using the number of points of the reconstructed shape. For the test, several percentages of points were considered (5 %, 10 %, 15% and 20%).

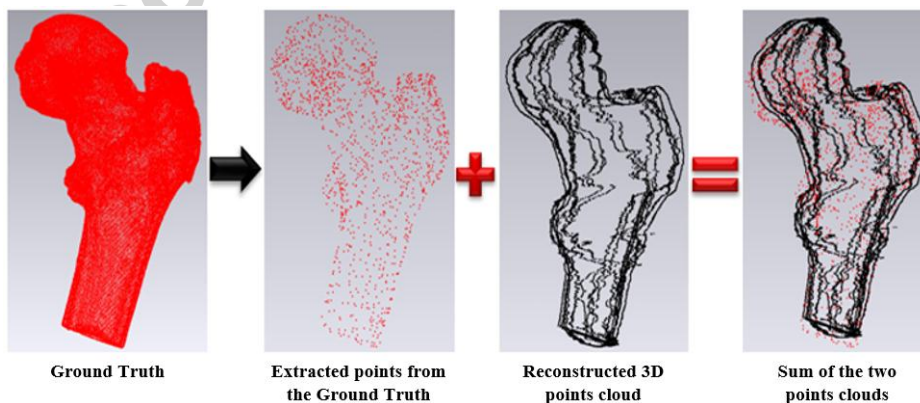


**Figure 9:** Illustration of the global approach: extraction of points from the GT shape to be injected inside the reconstructed shape.



To validate our approach, we used two proximal femurs, the volume CT-Scan of the proximal femur F1 as the reference volume and the proximal femur F2 as the volume to be reconstructed and vice versa (i.e. the proximal femur F2 as the reference volume and the femur F1 as the volume to be reconstructed). Before the extraction points, a registration was realized between the two femurs (3D reference surface and the reconstructed one). This way, we ensure that the two femurs are comparable in size and are set in the same environment. The results are shown in Table 4.

**Table 4:** Estimated errors for the proximal femurs F1 and F2 using the global approach.

Percentage of injected points	Maximum (mm)		Mean (mm)		RMS (mm)	
	F1	F2	F1	F2	F1	F2
0%	9.421	9.237	0.889	1.259	1.369	1.753
5%	9.241	8.791	0.906	1.296	1.359	1.728
10%	8.775	8.630	0.891	1.253	1.301	1.657
15%	8.654	7.491	0.933	1.207	1.328	1.592
20%	8.660	7.615	0.969	1.223	1.358	1.605

These results show that the estimated errors decrease with some percentage of injected points from the reference volume. This finding is consistent with our expectations. The maximum error also decreases substantially and the shape of the great trochanter is better reconstructed with less error. However, beyond 15% of injected points, the average and the RMS errors increase slightly. This is mainly due to the global shape of the reconstructed femur which conforms to the shape of the reference volume. This demonstrates the importance of combining the two approaches: stereo reconstruction and shape constraint by completing the reconstructed volume from a reference model [15].

### 3.3.2. Local correction

As the global approach constrains the reconstructed volume to conform to the shape of the reference volume, here we propose a new approach that consists in inserting points from a 3D reference shape only at specific locations that need to be improved. The targeted areas are those that reduce the precision of the reconstruction and increase the errors. These areas generate largest errors, because of occlusion problem. A semi-automatic procedure with human-machine interaction was adopted to reduce errors, thereby removing aberrant 3D

points and injecting in the same zones points from the 3D reference shape. To do so, first a 3D/3D registration is conducted to register the two 3D shapes in the same environment. Then, a 3D points cloud is extracted from the reference shape. The points to extract are selected massively by the operator from the targeted area. All the points are kept and then fused to the 3D shape to be reconstructed. Figure 10 shows the points extracted from the reference shape and inserted into the reconstructed shape.

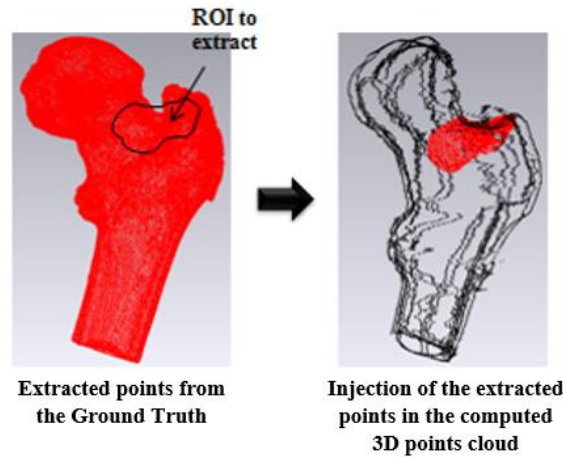


**Figure 10: Illustration of the local shape correction method.**

To validate our approach, we used the CT-Scan volume of the proximal femur F1 as the reference volume to reconstruct the proximal femur F2 and vice versa. The results obtained for the two proximal femurs F1 and F2 are shown in Table 5.

**Table 5:** Estimated errors for the reconstructed proximal femurs F1 and F2 using the local shape correction method.

	Maximum error (mm)		Mean error (mm)		RMS (mm)	
	F1	F2	F1	F2	F1	F2
No correction	9.421	9.237	0.889	1.259	1.369	1.753
Local shape correction method	<b>3.908</b>	<b>5.624</b>	<b>0.792</b>	<b>1.102</b>	<b>1.042</b>	<b>1.433</b>

These results show that targeting the areas to be improved reduces the errors and increases the precision of the 3D shape reconstruction.

## 4. CONCLUSION

In this paper, we have presented a new method for the 3D reconstruction of the femur shape from a relatively small number of X-ray projections. Our proposed method combines an X-ray stereo model and contour points matching. Cadaveric proximal femurs and their CT scans were used to assess the feasibility of our study.

This work shows that it is possible to reconstruct the 3D surface of the proximal femur from a relatively small number of X-ray projections with an average error of 0.89 mm and an RMS of 1.37 mm. The proposed reconstruction scheme combines an X-ray stereo model and shape constraint. The accuracy of the reconstructed shape was improved by using several 3D points extracted from a reference model obtained from CT-Scan images. The proposed technique to densify the 3D point cloud improves the results, since the average error and the RMS are reduced to 0.79 mm and 1.04 mm, respectively. Our proposed approach for 3D surface reconstruction of the proximal femur seems to be an interesting and promising technique. Further experiments using 2D classical X-ray images should be conducted to evaluate the effective potential of our method. For real clinical applications, a challenging point would be the contour extraction due to soft tissue and occlusion effects. As intra-operative assistance plays an important role in planning and supporting various computer assisted surgical procedures, we believe that our proposed approach is promising for clinical applications.

### **Competing interests:**

None declared

### **Ethical approval:**

Not required

### **Acknowledgment**

We gratefully acknowledge the Region Centre, France, for its support through the French APR Project (FRACTOS). The authors would also like to acknowledge Stéphanie Lerondel and Julien Sobilo from TAAM-CNRS UPS44 for the acquisition of the CT images.

## References

- [1] Gamage P, Xie SQ, Delmas P, Xu WL. Diagnostic radiograph based 3D bone reconstruction framework : Application to the femur. *Comput Med. Imaging Graph.* 2011; 35: 427-437.
- [2] Caponetti L, Fanelli AM. Computer-aided simulation for bone surgery. *IEEE Comput Graph Appl.* 1993; 13: 86-92.
- [3] Laporte S, Skalli W, De Guise JA, Lavaste F, Mitton D. A biplanar reconstruction method based on 2D and 3D contours: application to the distal femur. *Comput Methods Biomech Engin.* 2003; 6: 1-6.
- [4] Le Bras A, Laporte S, Bousson V, Mitton D, De Guise JA, Laredo JD, Skalli W. 3D reconstruction of the proximal femur with low-dose digital stereoradiography. *Comput Aided Surg.* 2004; 9: 51-57.
- [5] Baka N, Kaptein BL, de Bruijne M, van Walsum T, Giphart JE, Niessen WJ, Lelieveldt BPF. 2D-3D shape reconstruction of the distal femur from stereo X-ray imaging using statistical shape models. *Medical Image Analysis.* 2011; 15: 840-850.
- [6] Whitmarsh T, Humbert L, De Craene M, Del Rio Barquero LM, Frangi AF. Reconstructing the 3D Shape and Bone Mineral Density Distribution of the Proximal Femur From Dual-Energy X-Ray Absorptiometry. *IEEE Transactions on Medical Imaging.* 2011; 30: 2101-14.
- [7] Zheng G, Gollmer S, Schumann S, Dong X, Feilkas T. A 2D/3D correspondence building method for reconstruction of a patient-specific 3D bone surface model using point distribution models and calibrated X-ray images. *Medical Image Analysis.* 2009; 13: 883-899.
- [8] Baudoin A, Skalli W, de Guise JA, Mitton D. Parametric subject-specific model for in vivo 3D reconstruction using bi-planar X rays: application to the upper femoral extremity. *Med Biol Eng Comput.* 2008; 46: 799-805.
- [9] Chaibi Y, Cresson T, Aubert B, Hausselle J, Neyret P, Hauger O, de Guise JA, Skalli W. Fast 3D reconstruction of the lower limb using a parametric model and statistical inferences and clinical measurements calculation from biplanar X-rays. *Computer methods in biomechanics and biomedical engineering.* 2012; 15: 457-466.
- [10] Humbert L, de Guise JA, Aubert B, Godbout B, Skalli W. 3D reconstruction of the spine biplanar X-rays using parametric models based on transversal and longitudinal inferences. *Med Eng Phys.* 2009; 31: 681-687.
- [11] Boussaïd H, Kadoury S, Kokkinos L, Lazennec JY, Zheng G, Paragios N. 3D model based femur reconstruction of the proximal femur from low-dose biplanar X-ray images. *British Machine Vision Conference (BMVC'11).*
- [12] Zheng G, Schumann S. 3D reconstruction of a patient-specific surface model of the proximal femur from calibrated x-ray radiographs: a validation study. *Medical Physics.* 2009; 36: 1155-1166.
- [13] Feldkamp LA, Davis LC, Kress JW. Practical cone-beam algorithm. *Journal of the Optical Society of America A.* 1984; 1: 612-619.
- [14] Akkoul S, Hafiane A, Lespesailles E, Jennane R. 3D Femur Reconstruction Using X-ray Stereo Pairs. *International Conference on Image Analysis and Processing (ICIAP 2013), September 9-13th, 2013, Naples, Italy.*

- [15] Akkoul S, Hafiane A, Leconge R, Harrar K, Lespesailles E, Jennane R. 3D Reconstruction Method of the Proximal Femur and Shape Correction. International Conference on Image Processing Theory, Tools and Applications (IPTA 2014), October 14-17th, 2014, Paris, France.
- [16] Chan T, Vese L. Active contours without edges. IEEE Transaction on Image Processing. 2001; 10: 266-277.
- [17] Mumford D, Shah J. Optimal approximation by piecewise smooth function and associated variational problems. Communication on Pure and Applied Mathematics. 1989; 42: 577-685.
- [18] Akkoul S, Hafiane A, Leconge R, Lespesailles E, Jennane R. A 2D Matching Method for Reconstruction of 3D Proximal Femur using X-Ray Images. International Conference on Computer Vision, Imaging and Computer Graphics Theory and Applications (VISAPP 2013), February 21-24th, 2013, Barcelona, Spain.
- [19] Cui M, Femiani J, Hu J, Wonka P, Razdan A. Curve matching for open 2D curves. Journal Pattern Recognition Letters. 2009; 30: 1-10.
- [20] Frenkel M, Basri R. Curve matching using the fast marching method. Energy Minimization Methods in Computer Vision and Pattern Recognition. Lecture Notes in Computer Science. 2003; 2683: 35-51.
- [21] Park JS, Han JH. Contour matching: a curvature-based approach. Image and Vision Computing. 1998; 16: 181-189.
- [22] Besl PJ, McKay HD. A method for registration of 3-D shapes. IEEE Transactions on Pattern Analysis and Machine Intelligence. 1992; 14: 239-256.
- [23] Almhdie A, Léger C, Deriche M, Lédée R. 3D Registration Using a New Implementation of the ICP Algorithm Based on A Comprehensive Lookup Matrix : Application to Medical Imaging. Pattern Recognition Letters. 2007; 28: 1523-1533.
- [24] Andette M, Ferrie F, Peters T. An Algorithmic Overview of Surface Registration Techniques for Medical Imaging. Medical Image Analysis. 2000; 4: 201-217.
- [25] *Meshlab*, [meshlab.sourceforge.net](http://meshlab.sourceforge.net).
- [26] Cignoni P, Rocchini C, Scopigno R. Metro: measuring error on simplified surfaces. Computer Graphics Forum, Blackwell Publishers. 1998; 17: 167-174. Available at <http://vcg.sf.net>.
- [27] Kim K. j., Lee S. Kim Y. H., Dense femur reconstruction from two x-ray images using generic 3D model with twist correction. IEEE International Conference on Image Processing (ICIP), 2015, Quebec City, QC, pp. 3645-3649. doi: 10.1109/ICIP.2015.7351484.
- [28] Karade V, Ravi B. 3D femur model reconstruction from biplane X-ray images: a novel method based on Laplacian surface deformation. Int J Comput Assist Radiol Surg. 2015 Apr; 10(4):473-85. doi: 10.1007/s11548-014-1097-6. Epub 2014 Jul 19.
- [29] Yu W., Zysset P., Zheng G. Personalized x-ray reconstruction of the proximal femur via a non-rigid 2D-3D registration. Medical Imaging 2015: Image Processing, 94133B (March 20, 2015); doi:10.1117/12.2082339.
- [30] Kruskal J. B. On the shortest spanning subtree of a graph and the travelling salesman problem. Proceedings of the American Mathematical Society. 1956, 7: 48-50, Providence, United States, American Mathematical Society. doi:10.1090/S0002-9939-1956-0078686-7.

- [31] Tam G. K. L. et al. Registration of 3D Point Clouds and Meshes: A Survey From Rigid to Non-Rigid. IEEE TRANSACTIONS ON VISUALIZATION AND COMPUTER GRAPHICS, VOL. 19, NO. 7, JULY 2013.

### Highlights

- 3D reconstruction method of the proximal femur shape using few 2D radiographs
- New model based on the principle of stereo-radiography
- Development of a complete processing chain
- Global and local corrections models to improve the reconstructed 3D shape
- Results show good performances and promising prospects for 3D reconstruction of the proximal femur shape